A Novel Pulse-Coupled Neural Network using Gabor Filters for Medical Image Fusion

[1]**Fayadh Alenezi,** [2]**Ezzatollah Salari**

[1,2]Dept. of EECS, University of Toledo, Ohio, United States

Abstract

Medical image fusion is important in biomedical applications for non-invasive diagnosis. Image fusion aims to reduce defects associated with single images created from different modalities. These defects make the single-image result less informative and therefore less useful for medical diagnosis. An ideal fused image, created from two or more multimodality images, increases the accuracy, information content and improves visual properties. Current state-of-the-art image fusion techniques have not successfully resolved the poor visual properties, leading to less-than-ideal information quality. This paper describes a novel technique to improve information quality of fused images, with many practical applications in the biomedical, military, and remote sensing. The proposed algorithm combines the action of Gabor filtering, maximum pixel intensity selection and Pulse Coupled Neural Network (PCNN) implementation. The results are then used to create a fused image. As a proof of concept, several images are evaluated with standard criteria and compared with results from existing image fusion methods.

Keywords

Gabor Filter, Maximum Selection, PCNN, Imfuse, Imfilter, Medical Image Fusion.

I. Introduction

Image fusion is an important sub-field in image processing [1]. Single source images are often characterized by poor illumination and shift variance among other defects [2]. These defects result in images that are sub-optimal for human visual perception, limiting their use in critical applications. By fusing multiple images, each with their own features, image fusion techniques attempt to optimize the results. Fused images, combined from two or more source images, form a single image that is both more informative and better suited for human visual perception [3]. The improved information content and readability of fused images has resulted in widespread applications in areas such as medical imaging, satellite reconnaissance, military operations, and robotics.

These common applications includes multi-view, multi-modal, multi-temporal, or multi-focus fusion as well as fusion for image restoration. The corresponding algorithms typically use methodologies that capture image features at the signal, pixel, feature or decision level [4-5] and attempt to incorporate the information into the fused images. Many such techniques have limitations when operating on real images because they do not preserve anisotropic features, such as texture or edge clarity transforms [6], or they lack shift invariance and result in image distortion [7] or blocking effects [8].

More recent fusion techniques combiningContourlettransforms, Pulse Coupled Neural Networks (PCNN) and fuzzy logic have demonstrated some improved results [3, 6]. Several published studies have implemented PCNN to sort and filter source images before fusion [9-12] and demonstrated improved edges and textures

or contrast preservation in the resulting fusion. Other approaches are specialized in the way the PCNN is implemented, by using sub-netted PCNN components [13], by operating in a region-based schema [14], or by modifying the PCNN to automatically adjust its own linking coefficients [15-16]. These approaches are time-consuming and requirecomplex computations [4, 6, 17] and still lack the ability to take into account the characteristics of the Human Visual System (HVS). If optimized for human perception, results would take advantage of HVS improved edge completion and texture-recognition capabilities [9].

The proposed method uses Gabor filtering and maximum-intensity pixel selection through a PCNN to enhance the source images before fusion, aiming to preserve the sharpness of the images.

The remainder of the paper is organized as follows: Section II introduces the proposed method, giving a detailed explanation of the Gabor filtering and PCNN methods used. Section III discusses simulation resultsfrom a number of different Gabor Filter orientations. Section IVprovides conclusions which point in the direction of future research.

II. Proposed Method

A. Overview and Background

The proposed method,as illustrated in fig. 1, begins with Gabor filtering of two or more source images. Gabor filters are special classes of band-pass filters, which allow a certain 'band' of frequencies and reject the others. They can be implemented in either the spatial or frequency domain and are oriented in specific directions to preserve edges and textures [18].

Following Gabor filtering, a region-based fuzzy logic algorithm calculates the local maximum intensity for each pixel in each image. When these values are compared between source images, a mask (to be applied to one source image), and its inverse (to be applied to the other) are created to pass through only the Maximum pixel value. The masking process guarantees that no compromise need be made in separating noise from useful information contained in the resultant Gabor filter images.

The masked images are then used as input to the Pulse Coupled Neural Network (PCNN). PCNN is a self-organizing network that does not require training [15]. PCNN has the ability to extract relevantinformation from a complex background in an iterative fashion [29]. The general model for PCNN methodology was developed by Eckhorn based on practical observations of the synchronous pulse burst in visual cortices of cats and monkeys [17]. PCNN is characterized by global coupling and pulse synchronization of neighboring neurons which share locally enhanced action potentials through neuronal linking mechanisms. The ability of PCNN to couple and synchronize neurons makes it adaptable and easily optimized for image processing applications such as image fusion [20].
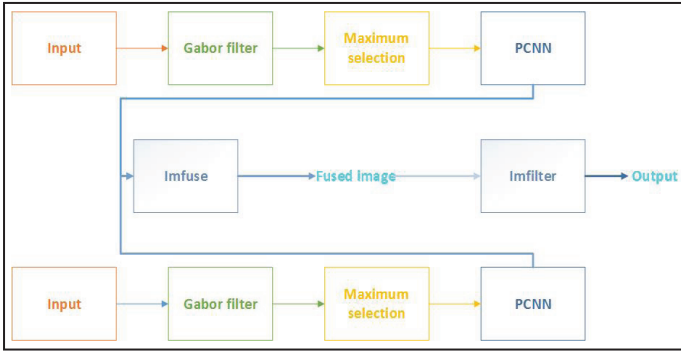
Fig. 1: Schematic Representation of Novel Algorithm Combining Gabor Filtering, Masking to Select the Local Maximum Pixel Intensities, and PCNN Image Enhancement, Followed by Image Fusion.

The PCNN typically used in image processing applications consists of three stages: the input feed (feedforward); the linking feed (feedbackward), which modulates the input; and the pulse generator, which yields the result [17]. These stages are described in equations1a-e, and illustrated in fig. 2. The feeding inputat each iteration, F_{ij} (n), is the masking result for each pixelwith position indices i,j (1a). In the feeding input, S_{ij} is the input image value in grayscale. The linking input (1b) is derived from previous linking values and a combination of neighborhood results from the previous iteration

$$F_{ij}(n) = S_{ij} \qquad (1\ a)$$

$$L_{ij}(n) = exp(-\alpha_L)\, L_{ij}(n-1) + V_L \sum_{kl} W_{ijkl} Y_{kl}(n-1) \quad (1\ b)$$

$$U_{ij}(n) = F_{ij}(n)\left(1 + \beta L_{ij}(n)\right) \qquad (1\ c)$$

$$\theta_{ij}(n) = exp(-\alpha_\theta)\, \theta_{ij}(n-1) + V_\theta Y_{ij}(n) \qquad (1\ d)$$

$$Y_{ij}(n) = \begin{cases} 1, & \forall\ U_{ij}(n) > \theta_{ij}(n); \\ 0, & \forall U_{ij}(n) \le \theta_{ij}(n); \end{cases} \qquad (1\ e)$$

Where n, is the time index of the iterations, while $(\alpha_L, \alpha_\theta)$ are time attenuation constants for link inputs and (V_L, V_θ) are normalization constants for dynamic thresholds, W_{ijkl} are the neighborhood weighting values, and Y_{kl} (n-1) are results of the previous iteration within the neighborhood(denoted in the equation by the subscripts 1). L_{ij} (n)(1b) and Y_{ij} (n)(1e) are combinations of these values used during linking and pulse generation stages as illustrated in fig. 2.

Input values to each neuron consist of Y_{kl},which is the output from Maximum value selection, and Y_{ij}, pulse output from neighboring neurons. The nonlinear modulation stage, with weighted linking constants β_{ij} results in values U_{ij}, which are compared to the dynamic firing thresholds θ_{ij}. When thresholds are exceeded, a neuron fires.
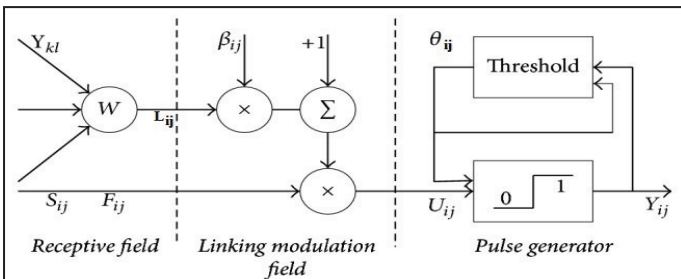

Fig. 2: One Neuron in a Neural Network Consisting of Input, Linking and Generator stages

The details of the proposed implementation of PCNN, which is slightly different, are described in Section IIC and illustrated fig. 3.

The output from PCNN becomes the input to the fusion function, Imfuse, followed by Imfilter. Both functions are part of the Matlab image processing toolbox (Matlab 2016b). In this paper, we use PCNN to extract image features; PCNN also can extract the information of the image's texture, edge and regional distribution and has a good effect on image processing. Imfuse is a function, which rectifies input images of different sizes by padding and allowing for spatial referencing to account for variations in voxel dimensions and Field Of View (FOV) without resampling pixel intensities [21]. This capability is useful when fusing multimodality medical images, which often have inherently different image resolution and FOV. The Imfuse outputs for each source image are then placed in different color channels of a multidimensional array, which is slightly smoothed, without losing texture detail, using Imfilter. This produces the final image, examples of which will be shown later.

B. Gabor filtering

Gabor filters possess optimal localization properties in both the spatial and frequency domains, while being useful for removing noise and enhancing visual features and edges [22]. They are invariant to illumination, rotation, scaling and translation because they operate as sinusoidal planes within a Gaussian envelope [23].

In our proposed method, they are applied to the source images in order to enhance textural properties [24]. The 2-D Gabor function is described by the following equations:

$$g_{\lambda,\theta,\varphi,\sigma,\gamma}(x,y) = \exp\left(\frac{x'^2 + \gamma^2 y'^2}{2\sigma^2}\right) \cos\left(\frac{2\pi x'}{\lambda} + \varphi\right), \quad (2)$$

where

$$x' = x\cos\Theta + y\sin\Theta,$$

$$y' = -x\sin\Theta + y\cos\Theta.$$

λ(which is set to 3.5) is the wavelength of the sinusoidal factor, Θ is the degrees of orientation of the filter, φ is the phase, σ is the standard deviation of the Gaussian envelope, and γ is the aspect ratio [9, 19].

The optimum parameters chosen for the Gabor filter in this study(determined by measurements of root mean square error (RMSE), standard deviation (SD), and entropy, to be discussed in the results section, are as follows: the filter is set to a 10x10 size with a given*ktype* (a classification of type and range of values (0-255) at each position in the Gabor kernel). The orientation angles (θ), 0, 90, 180 and 270 degrees are considered, with γ=1.25, ψ=0, λ=3.5, and a bandwidth value of 2.8 (ratio of standard deviation of the Gaussian function and the preferred wavelength).

C. Proposed PCNN

The proposed PCNN model shown in fig. 3 is slightly different from the general PCNN model. In this case, a linking synapse is inspired by the γ band synchronization and dynamic threshold. As shown in fig. 1, a neuron has feeding synapses and lateral linking synapses. Feeding synapses are connected to a spatially corresponding stimulus, and lateral linking synapses are connected to outputs of neighboring neurons within a predetermined radius. Locally excitatory linking inputs have a negative globally inhibitory term that supports desynchronization [27-28] is designed to simulate the refractory period of a neuron [29].
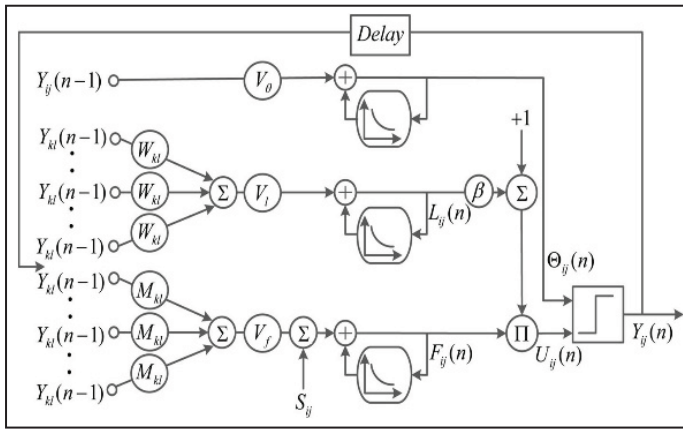
Fig. 3: Schematic Representation of Classical PCNN, Using Eight Scalar Parameters: α_f, V_f, α_l, V_l, α_θ, V_θ, β and n.

As with traditional PCNN, the proposed PCNN also has 3 scalar variables (n,i , and j), and 5 matrix variables, (F_{ij} (n), L_{ij} (n), U_{ij} (n), Y_{ij} (n) and Θ_{ij} (n)) wheren(n∈[0,N]) is a time variable, while (i,j) are spatial coordinate variables [30].

The central terms of the membrane potential of the PCNN, in fig. 3, are attained by assuming the linking strength β set to a value close to zero. In our method, β is set to 0.5 while the convolution kernel in the feeding input is also set to values of 0.111. The resultant membrane potential is then given by [30],

$$U_{ij}(n) = f U_{ij}(n-1) + S_{ij} \qquad (3)$$

f is a constant describing the relationship between values in the sequence. By rearranging equation (3), U_{ij} (n) can be expressed in terms of the initial values as:

$$U_{ij}(n) = \left(U_{ij}(0) - \frac{S_{ij}}{1-f}\right) f^n + \frac{S_{ij}}{1-f}. \qquad (4)$$

Where f = exp(-α_θ) (from equation 3) is a simplification for ease of understanding and 0<f<1.

The resulting characteristics of the PCNN operation are as follows, and described further in sections 1-4. The network is designed to be self-terminating, after a single-pass, where each neuron has generated an action potential only once. The firing rate of neurons in the network is governed by an iterative dynamically adjusted threshold to ensure that a neuron with a strong stimulus will fire before a neuron with weak stimulus. This firing pattern is also synchronized within a local neighborhood, and is governed by the linking inputs. The combined effect of all these mechanisms is that visual properties are enhanced by the PCNN action in the proposed image fusion method.

1. Single-pass
A single-pass is a complete iteration of the PCNN time matrix used to extract visual properties for enhancement and edge completion, as described by (2) [29]. A single-pass is completed when all the neurons have generated an action potential V_θ, which is set to higher values to excite neurons to generate the action potential only once [31]. In our method, the threshold amplification factor V_θ is set to 20, high enough that the iterative process will stop automatically when all neurons have fired once, so that a complete time series has been collected [29].

2. Firing Rate
Assuming the membrane potential is equal to the stimulus, the precise firing time occurs when the membrane potentialis almost equivalent to the dynamic threshold (performance alerts are generated based on a dynamic baseline generated by the system):

$$\Theta_{ij}(n) = S_{ij} \qquad (5)$$

Sub sequential firing activity will update the dynamic threshold in the next iteration according to:

$$\Theta_{ij}(n+1) = g\Theta_{ij}(n) + V_\theta = gS_{ij} + V_\theta \qquad (6)$$

where g= exp(-α_θ) (from equation 1d) is a simplification for ease of understanding and 0<g<1.

The value of the thresholddecreases exponentially from its initial value Θ_{ij} (0) at first firing time, and is delayed at each subsequent firing according to the value $gS_{ij} + V_\theta$. By rearranging equation (6), and substituting g= exp(-α_θ), it is possible to express the value of n in terms of the other parameters, as given in equation (7):

$$n = \log_g \frac{S_{ij}}{\Theta_{ij}(0)} + \sum_{n>1} \log_g \frac{S_{ij}}{gS_{ij}+V_\theta} \qquad (7)$$

Assumingthat the membrane potential is constant for a single neuron and that its analytical solution is an approximation based on the firing frequency F_{ij},

$$\mathcal{F}_{ij} = \frac{1}{\log_g \frac{S}{gS_{ij}+V_\theta}} \qquad (8)$$

It can be shown that a neuron with a strong stimulus is fired earlier than a neuron with weak stimulus [30]. Neurons with weak stimuli are the last to be fired.

3. Synchronization
The proposed method also incorporates stimulus-induced synchronization which is related to the linking wave [26]. The linking wave spreads in a circle from a central neuron, while radii of the wave increase step by step, coupling all the neurons in the neighborhood so that they fire synchronously. The linking wave then preferentially selects neurons whose stimuli are similar to the previously fired neuron [19].

4. Visual Properties Enhancement
Pulse synchronization in PCNN enables image property enhancement through its time matrix [25], because the membrane potential is approximately equal to the stimuluswhen neurons fire. Let time T_ijbe the time when the membrane potential exceeds its threshold, and let this time correspond to iteration n. In other words, neuron (i,j) fires at the time T_{ij} when the membrane potential $U_{ij}(T_{ij})$ is only slightly greater than its threshold $\Theta_{ij}(T_{ij}) = g(T_{ij})$ $\Theta_{ij}(0)$, hence $U_{ij}(T_{ij}) \cong g^{T_{ij}}$ $\Theta_{ij}(0)$. Therefore, the firing time T_{ij} will be given by

$$T_{ij} = \log_g S_{ij} - \log_g \Theta_{ij} \qquad (9)$$

The time matrix represented in (9) corresponds to Weber-Fechner's law, and has an approximate logarithmic relation with the stimuli matrix. Thus, neurons with a larger stimulus fire first before neurons with a smaller stimulus [19]. The resulting image exhibits enhanced visual properties, with improved contrast and preserved edges and texture of the images.

III. Simulation Results

A. Experimental Setup

Three different examples, presented in fig. 4, 5, and 6,are used to evaluate the proposed method. The Gabor filters were orientedin fourdirections, $\theta = 0^0$, 90^0,180^0, and 270^0. PCNN parameters are defined in Table 1. The final results were evaluated using objective quantitative measurements: standard deviation, root mean square error (RMSE) and entropy. These were selected based on their use as descriptors of textural properties, information content and Signal-to-noise ratio (SNR). These descriptors were also used as measurements in previously published results for other fusion methods enabling us for a common comparison. Standard deviation is a measure of the contrast, textual properties, and edge formation of the image. Images with high standard deviation have better improved human visual properties (textual properties and better edge formation). RMSE measures the amount of change per pixel due to processing. Lower RMSE is an indication of lower noise levels in the image and thus improved visual features. Entropy measures image quality in terms of information content [33]. Therefore, images with higher entropy contain more information. Entropy measures image qualities in terms of textural uniformity and is thus a preferable metric of quality for fused medical images.

This measure contains more textural properties making them more effective in terms of fusion [25].

The example images and results as shown in Figs. 4, 5, and 6, yielded measurements presented in Tables 2, 3, and 4. The best results were then compared with measurements from previously published (existing) techniques. Comparison results are presented in Table 5 and fig. 7, with summary bar graphs in figs. 8, 9, and 10.

Table 1: List of PCNN Parameters Values Used for Experiments 1, 2 and 3

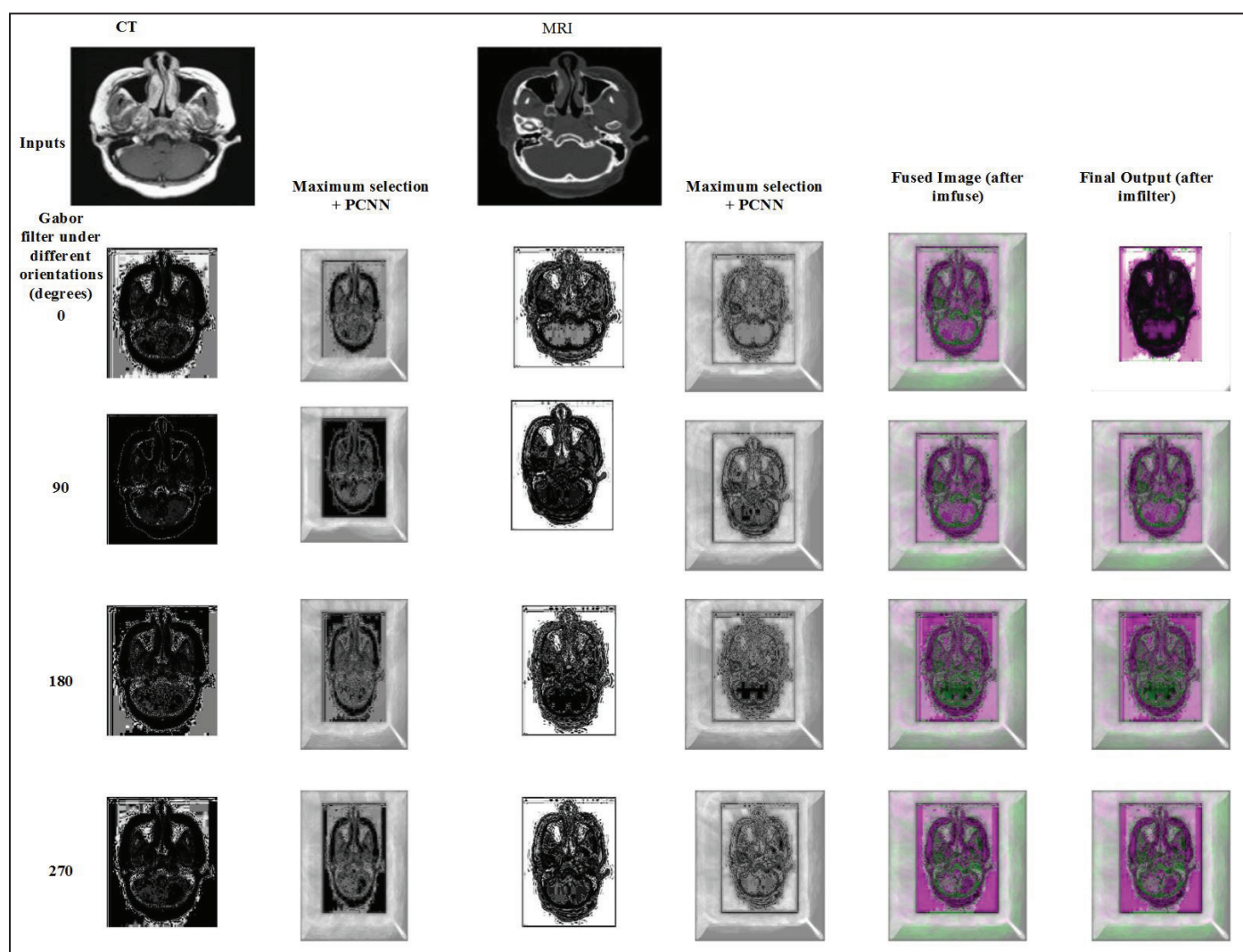| Parameter	Value used
α_L	1
α_θ	0.2
β	0.5
V_L	1
V_θ	20
Link arrangement	16
Iteration times	250

Fig. 4: Example 1: Inputs are CT and MRI images asshown in Row 1. Gabor filter results at different orientations (θ is 0, 90, 180 and 270 degrees) areshown in column 1 and 3, with corresponding maximum value selection results in columns 2 and 4. The results of fusion (imfuse output), and the final fused image (imfilter output) are shown in columns 5 and 6.
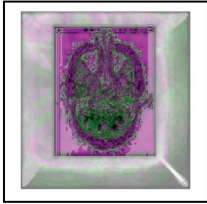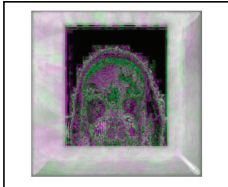
Table 2: Performance Evaluation Measures for Example 1 (Fig. 4) Under Different Orientations of Gabor Filtering

Performance evaluation measures	Values at different directions (θ)			
	0°	90°	180°	270°
Entropy	8.9867	9.0049	9.1595	9.1559
Standard deviation	50.0335	63.0644	57.3573	53.3573
RMSE	0.0177	0.0173	0.0193	0.0187
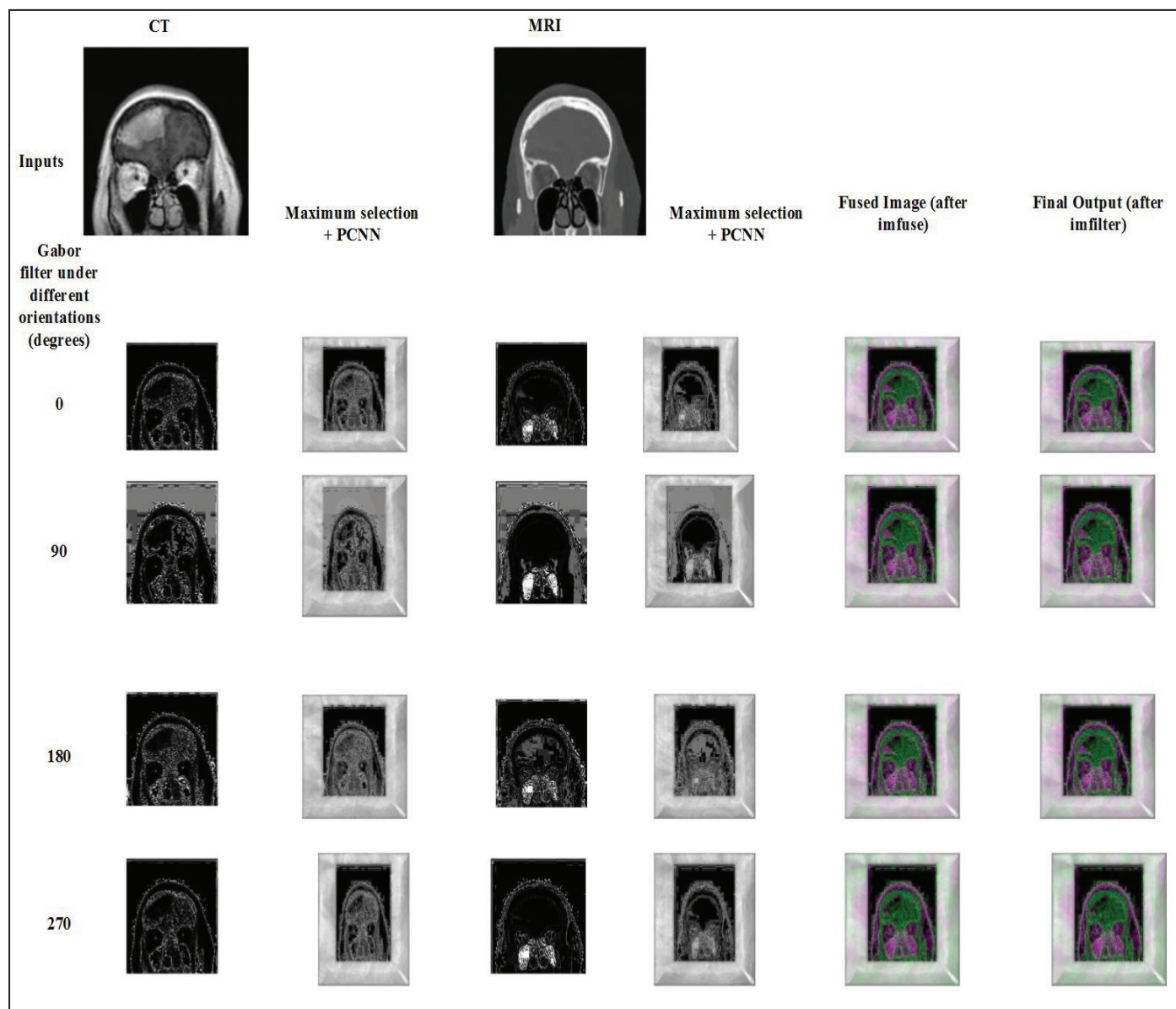
Fig. 5: Example 2: Inputs are CT and MRI images as shown in Row 1. Gabor filter results at different orientations (θ is 0, 90, 180 and 270 degrees) are shown in column 1 and 3, with corresponding maximum value selection results in columns 2 and 4. The results of fusion (imfuse output), and the final fused image (imfilter output) are shown in columns 5 and 6.
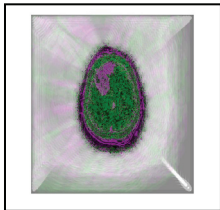
Table 3: Performance Evaluation Measures for Example 2 (Fig. 5) under Different Orientations of Gabor Filtering

Performance evaluation measures	Values at different directions (θ)			
	0°	90°	180°	270°
Entropy	8.8606	8.7162	8.9667	8.9273
Standard deviation	77.6431	61.3606	71.6609	76.7252
RMSE	0.0178	0.0153	0.0187	0.0188
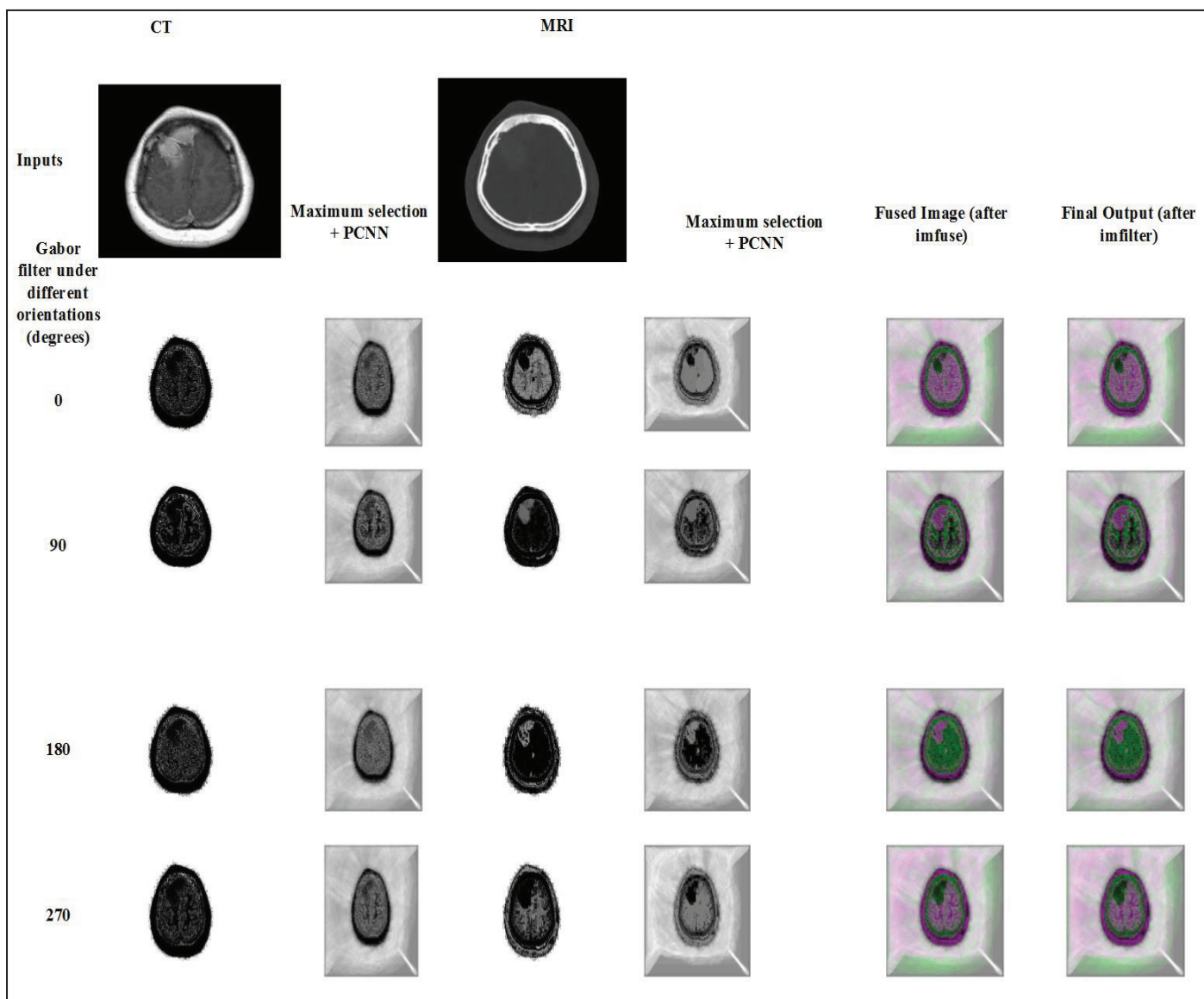
Fig. 6: Example 3: Inputs are CT and MRI images asshown in Row 1. Gabor filter results at different orientations (θ is 0, 90, 180 and 270 degrees) are shown in column 1 and 3, with corresponding maximum value selection results in columns 2 and 4. The results of fusion (imfuse output), and the final fused image (imfilter output) are shown in columns 5 and 6.

Table 4: Performance Evaluation Measures for Example 3 (Figure 6) under different orientations of Gabor filtering

Performance evaluation measures	Values at different directions (θ)			
	0⁰	90⁰	180⁰	270⁰
Entropy	8.3932	8.7063	8.7121	8.6019
Standard deviation	49.7551	55.4118	56.8493	52.6867
RMSE	0.0123	0.013	0.014	0.0125

Table 5 and fig. 7 describe the performance of the proposed algorithm in comparison with some other methods including Contourlet Transform (CT) [25]; Discrete wavelet transform (DWT) [25]; Shearlets and Human Feature Visibility (SHFV) [25]; and Fuzzy-Based using Maximum Selection and Gabor filters (FMG) [26]. Measures for comparison are Entropy, SD, and RMSE, taken from the sources referenced in column 6 in Table 5. Figs. 8, 9 and 10 are graphs which highlight the improved performance of the proposed method for each example with respect to each of the measures.

Table 5: Comparison of Image Quality Metrics for Fusion Algorithms.

Examples	Algorithm	Entropy	Standard Deviation	RMSE	Source
	Proposed method (Example 1)	9.1595	57.3573	0.0193	
	CT	7.1332	54.1504	0.1662	[25]
	DWT	6.9543	47.2304	0.2703	[25]
	SHFV	7.6572	56.7993	0.1164	[25]
	FMG	3.4507	117.7324	0.0736	[26]
	Proposed method (Example 2)	8.9667	71.6609	0.0187	
	CT	6.9351	46.6294	0.2538	[25]
	DWT	6.6997	41.4623	0.2889	[25]
	SHFV	7.3791	55.8533	0.2410	[25]
	FMG	3.8054	118.0412	0.1026	[26]
	Proposed method (Example 3)	8.7121	56.8493	0.014	
	CT	6.8824	43.1963	0.2422	[25]
	DWT	6.5198	42.0087	0.3142	[25]
	SHFV	6.9467	44.2937	0.2133	[25]
	FMG	2.3886	94.6862	0.0774	[26]
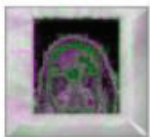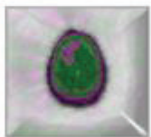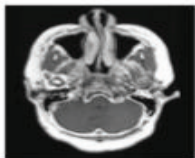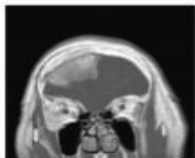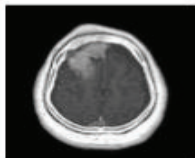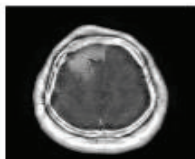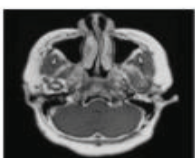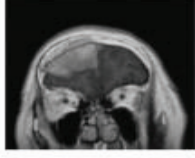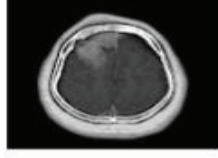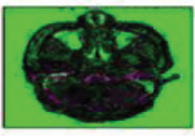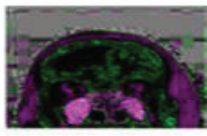
Fig. 7: Fusion Results on Test Original Multimodality Image Dataset 1, 2, and 3 Using Proposed Method, CT, DWT, SHFV, and FMG.

A graphical representation of the performance of our proposed method in relation to the existing methods is also portrayed in the graphs in Fig. 8, 9, and 10.
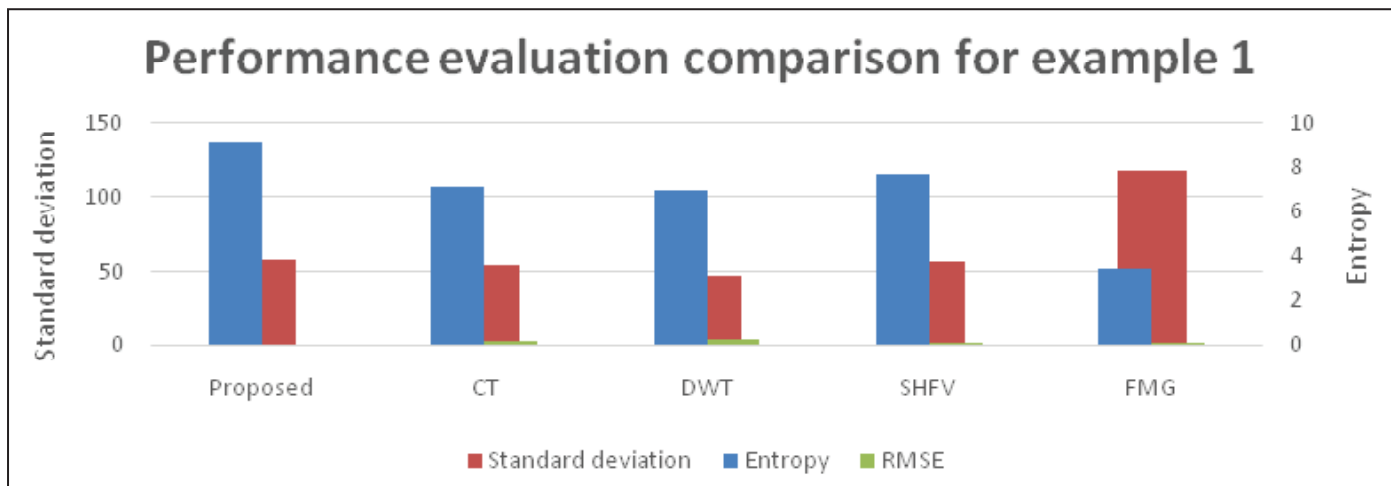

Fig. 8: Bar Graph Highlighting the Performance of the Proposed Method in relation to others for Example 1 (Fig. 4).
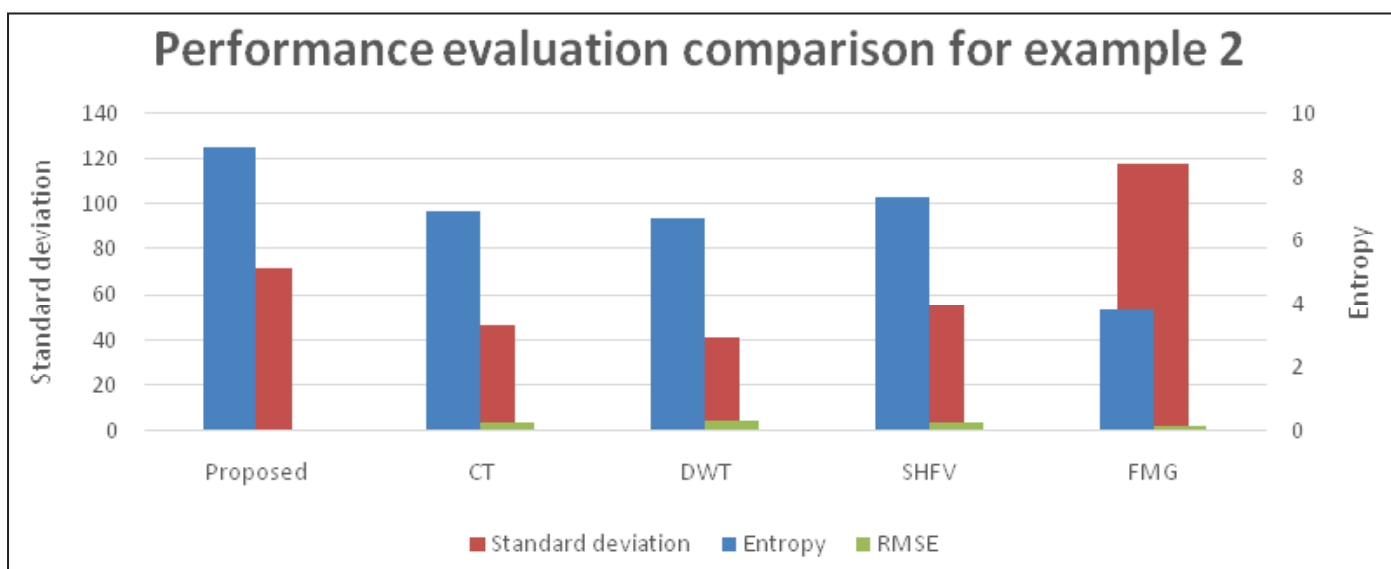

Fig. 9: Bar Graph Highlighting the Performance of the Proposed Method in Relation to others for Example 2 (Fig. 5)
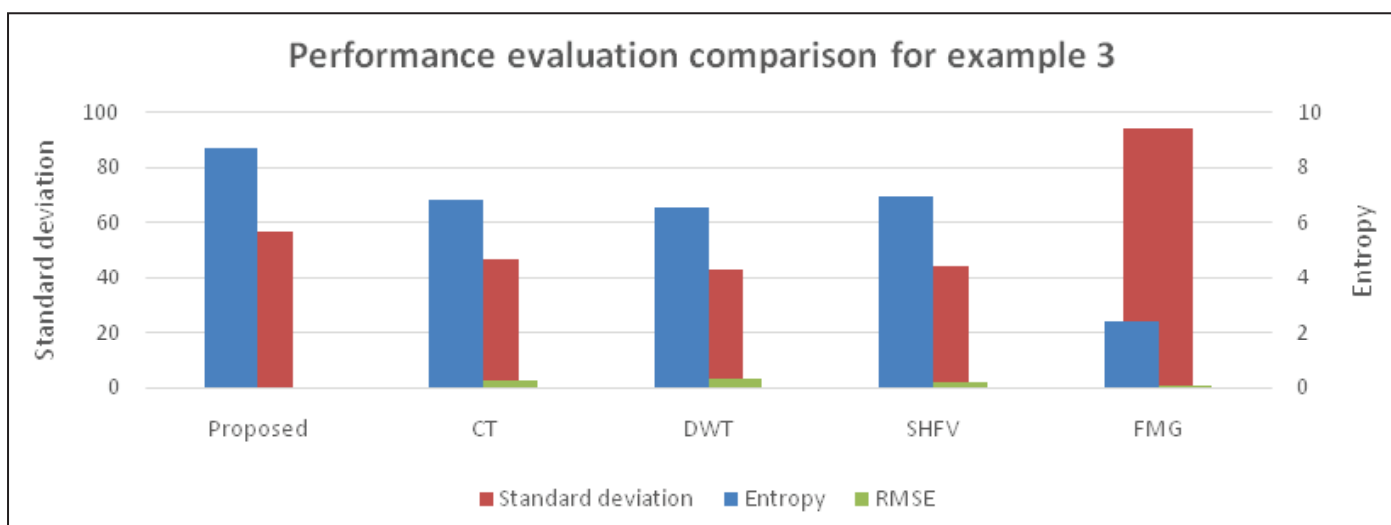

Fig. 10: Bar graph highlighting the performance of the proposed method in relation to others for Example 3 (Fig. 6)

B. Discussion

Image fusion is very important in data visualization. Medical image fusion, in particular, is critical in clinical medicine for non-invasive diagnosis. Human visual properties, in the form of textural properties and completeness in edge formation, have proven to be vital for medical images. Therefore, any medical image fusion technique must preserve the visual properties of fused images.

The proposed method demonstrates significant improvements over previously published methods for fusion. As summarized in Figure 8, resulting fused images show improved textural properties and edge information, as measured by SNR and RMSE.

A close analysis of the Entropy values, summarized for all examples in Table 5, confirms that our method has better information content than existing techniques most often. We must consider that the overall improvements to textural properties, edge formation, and information content are remarkable.

Although the proposed method has yielded improved results in most cases, the results produced mixed results in some other cases. RMSE results presented in Table 5 are consistent, i.e., all the values are the lowest in all examples. The lowest RMSE values are exhibited by highest SNR due to the Gabor filtering of the input images, maximum selection of the Gabor-filtered images, and final filtering of the fused images. The high standard deviation is also a result of Gabor filtering input images. FMG algorithm in Table 5 shows highest values of standard deviations. The FMG method entailed double Gabor filtering as each input image was Gabor filtered, which explains the highest standard deviations measurements. In our method, the input images are first Gabor filtered and then the fused image is slightly smoothed with Imfilter. Consequently, the standard deviation of the results is lower than those of the FMG method, but improved when compared to others. The rest of the existing methods did not employ Gabor filtering, but used other techniques. PCNN also has an impact on the measured values. The implementation seems to reduce loss of texture during fusion by including a local neighborhood within the linking phase. The end result is increased SNR, and lower RMSE, with higher information content measured by high entropy compared to other techniques.

IV. Conclusion

This paper presented a novel medical image fusion technique, based on PCNN coupled with Gabor filtering and maximum selection with smoothing of the fused image. The previously existing image fusion techniques produced mixed results based on the defined performance evaluation criteria. These methods have not yielded images with high information content or adequate visual properties i.e., improved textural properties and edge information, both of which are critical in clinical diagnosis. The proposed method presents fused images with better information quality and improved visual properties by exploiting the action of PCNN on images, maximum selection of pixels, and the properties of Gabor filtering. Based on the objective performance evaluation criteria, our method significantly outperforms leading-edge image fusion methods by making novel use of PCNN in combination with Gabor filtering.

Future studies should be conducted to show the effects of the proposed method when PCNN enhanced images are fused without Gabor filtering or maximum selection, to determine the effect of Gabor filtering of input images before enhancing the images using PCNN.

References

[1] A. Anish, T. J. Jebaseeli, "A Survey on Multi-Focus Image Fusion Methods," International Journal of Advanced Research in Computer Engineering & Technology (IJARCET), Vol. 1, No. 8, pp. 319, 2012.

[2] N. Nahvi, O. C. Sharma, "Comparative Analysis of Various Image Fusion Techniques For Biomedical Images: A Review," Engineering Research and Applications, Vol. 4, No. 5, pp. 81-86, 2014.

[3] L. Xu, J. Du, Q. Li, "Image fusion based on nonsubsampled contourlet transform and saliency-motivated pulse coupled neural networks," Mathematical Problems in Engineering, Vol. 2013.

[4] Y. Ma, K. Zhan, Z. Wang, "Applications of Pulse-Coupled Neural Networks, Heidelberg-New York: Springer, 2010.

[5] J. R. Suthakar, A. D. S. S. R. Monica E. M. E., "Study of Image Fusion- Techniques, Method and Applications," International Journal of Computer Science and Mobile Computing (IJCSMC), Vol. 3, No. 11, pp. 469-476, 2014.

[6] F. Liu, J. Li, H. Caiyun, "Image fusion algorithm based on simplified PCNN in nonsubsampled contourlet transform domain", Procedia Engineering, Vol. 29, pp. 1434-1438, 2012.

[7] Q. Zhang, B.-l. Guo, "Multifocus image fusion using the nonsubsampled contourlet transform", Signal processing, Vol. 89, No. 7, pp. 1334-1346, 2009.

[8] R. Maruthi, I. Lakshmi, "Multi-Focus Image Fusion Methods – A Survey," Computer Engineering, Vol. 19, No. 4, pp. 9-25, 2017.

[9] R. P. Broussard, S. K. Rogers, "Physiologically motivated image fusion using pulse-coupled neural networks," In Applications and science of artificial neural networks II, 1996.

[10] E. P. Blasch, "Biological information fusion using a PCNN and belief filtering," In Neural Networks, 1999. IJCNN'99. International Joint Conference on, 1999.

[11] B. Xu, Z. Chen, "A multisensor image fusion algorithm based on PCNN," In Intelligent Control and Automation, 2004. WCICA 2004. Fifth World Congress on, 2004.

[12] W. Li, X.-F. Zhu, "A new image fusion algorithm based on wavelet packet analysis and PCNN," In Machine Learning and Cybernetics, 2005. Proceedings of 2005 International Conference on, 2005.

[13] J. Y. Zhang, J. L. Liang, "Image fusion based on pulse-coupled neural networks," Computer Simulation, Vol. 21, No. 4, pp. 102-104, 2004.

[14] M. Li, W. Cai, Z. Tan, "A region-based multi-sensor image fusion scheme using pulse-coupled neural network," Pattern Recognition Letters, Vol. 27, No. 16, pp. 1948-1956, 2006.

[15] Z. Wang, Y. Ma, "Medical image fusion using m-PCNN," Information Fusion, Vol. 9, No. 2, pp. 176-185, 2008.

[16] Z. Wang, S. Wang, Y. Zhu, Y. Ma, "Review of image fusion based on pulse-coupled neural network," Archives of Computational Methods in Engineering, Vol. 23, No. 4, pp. 659-671, 2016.

[17] A. Wang, J. Zhao, S. Dai, Y. Z. Y. Iwahori, "Medical Image Fusion based on Pulse Coupled Neural Network Combining with Compressive Sensing," International Journal of Signal Processing, Image Processing and Pattern Recognition, Vol. 8, No. 5, pp. 223-230, 2015.

[18] Y. Yang, S. Tong, S. Huang, P. Lin, "Log-Gabor energy based multimodal medical image fusion in NSCT domain," Computational and mathematical methods in medicine, Vol. 2014, 2014.

[19] W. Xia, S. Yin, P. Ouyang,"A high precision feature based on LBP and Gabor theory for face recognition," Sensors, Vol. 13, No. 4, pp. 4499-4513, 2013.

[20] E. J. Candes, J. Romberg, T. Tao,"Robust uncertainty principles: Exact signal reconstruction from highly incomplete frequency information," IEEE Transactions on information theory, Vol. 52, No. 2, pp. 489-509, 2006.

[21] J. L. Semmlow, B. Griffel,"Biosignal and medical image processing", CRC press, pp. 394, 2014.

[22] V. S. N. Prasad, J. Domke,"Gabor filter visualization," J. Atmos. Sci, Vol. 13, p. 2005, 2005.

[23] V. Kyrki, J.-K. Kamarainen, H. Kalviainen,"Simple Gabor feature space for invariant object recognition", Pattern recognition letters, Vol. 25, No. 3, pp. 311-318, 2004.

[24] H. Yang, Y. Fang, W. Lin,"Perceptual quality assessment of screen content images", IEEE Transactions on Image Processing, Vol. 24, No. 11, pp. 4408-4421, 2015.

[25] N. A. Al-Azzawi,"Medical Image Fusion based on Shearlets and Human Feature Visibility", International Journal of Computer Applications, Vol. 125, No. 12, pp. 1-12, 2015.

[26] F. Alenezi, E. Salari,"A Fuzzy-Based Medical Image Fusion Using a Combination of Maximum Selection And Gabor Filters," International Journal of Scientific & Engineering Research, Vol. 9, No. 3, pp. 118-129, March 2018.

[27] R. Eckhorn, H. J. Reitboeck, M. T. Arndt, P. Dicke, "Feature linking via synchronization among distributed assemblies: Simulations of results from cat visual cortex", Neural computation, Vol. 2, No. 3, pp. 293-307, 1990.

[28] A. S. French, R. B. Stein,"A flexible neural analog using integrated circuits", IEEE Transactions on Biomedical Engineering, No. 3, pp. 248-253, 1970.

[29] J. L. Johnson, M. L. Padgett,"PCNN models and applications," IEEE transactions on neural networks, Vol. 10, No. 3, pp. 480-498, 1994.

[30] K. Zhan, J. Shi, H. Wang, Y. Xie, Q. Li,"Computational mechanisms of pulse-coupled neural networks: a comprehensive review," Archives of Computational Methods in Engineering, Vol. 24, No. 3, pp. 573-588, 2017.

[31] K. Zhan, H. Zhang, Y. Ma,"New spiking cortical model for invariant texture retrieval and image processing," IEEE Transactions on Neural Networks, Vol. 20, No. 12, pp. 1980-1986, 2009.

[32] V. P. S. Naidu, J. R. Raol,"Pixel-level image fusion using wavelets and principal component analysis", Defence Science Journal, Vol. 58, No. 3, pp. 338, 2008.

[33] K. Singh, R. Kapoor,"Image enhancement using exposure based sub image histogram equalization", Pattern Recognition Letters, Vol. 36, pp. 10-14, 2014.

[34] H. S. Ranganath, G. Kuntimad, J. L. Johnson,"Pulse coupled neural networks for image processing", In Southeastcon'95. Visualize the Future, Proceedings., IEEE, 1995.

[35] R. Eckhorn, H. J. Reitboeck, M. T. Arndt, P. Dicke, "Feature linking via synchronization among distributed assemblies: Simulations of results from cat visual cortex", Neural computation, Vol. 2, No. 3, pp. 293-307, 1990.

[36] J. L. Johnson, M. L. Padgett,"PCNN models and applications," IEEE transactions on neural networks, Vol. 10, No. 3, pp. 480-498, 1999.

[37] B. Yang, Z. Jing, H.-t. Zhao,"Review of pixel-level image fusion," Journal of Shanghai Jiaotong University (Science), Vol. 15, pp. 6-12, 2010.